ACS APPLIED ELECTRONIC MATERIALS

pubs.acs.org/acsaelm

Article

Studies of Atomic-Layer-Deposited $Zn_{1-X}Sn_XO_Y$ as an Alternative Buffer Layer for $Cu_2Zn(Sn_{1-X},Ge_X)S_4$ Thin-Film Solar Cells

Melike Babucci,* Tobias Törndahl, Soham Mukherjee, Charlotte Platzer Björkman, and Natalia M. Martin*

Cite This: *ACS Appl. Electron. Mater.* 2024, 6, 7989−7999

Read Online

ACCESS | Metrics & More | Article Recommendations | Supporting Information

ABSTRACT: Thin-film solar cells based on $Cu_2Zn(Sn_{1-X},Ge_X)S_4$ (CZTGS) absorbers are emerging technologies for solar energy conversion with low-cost, nontoxic components. In this work, we investigated CZTGS-based solar cells with varying Ge contents and an alternative buffer layer of $Zn_{1-X}Sn_XO_Y$ (ZTO) by atomic layer deposition. The results are compared to those of devices with the traditional CdS buffer layer. Overall, higher efficiency and open-circuit voltage (V_{OC}) are observed for the devices with ZTO compared to those with the CdS buffer layer. Moreover, the results show that the CZTGS/ZTO device performance may further be improved by varying the ZTO properties (band gap or thickness) or by applying a surface treatment on the CZTGS absorber. An air annealing treatment of the chemically etched absorber surface improved the CZTGS device performance; however, nonetched devices show poor efficiency due to the presence of secondary phases (GeO_2) at the absorber/buffer interface, shown by hard X-ray photoelectron spectroscopy measurements, as previously reported for the full-germanium Cu_2ZnGeS_4-based devices.

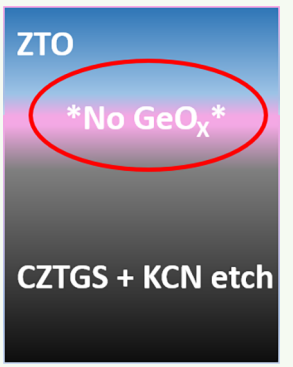

KEYWORDS: *atomic-layer-deposited $Zn_{1-X}Sn_XO_Y$ (ALD ZTO), hard X-ray photoelectron spectroscopy (HAXPES), $Cu_2Zn(Ge,Sn)S_4$ (CZTGS) absorbers*

INTRODUCTION

Thin-film solar cells based on kesterite Cu_2ZnSnS_4 (CZTS) semiconductors have emerged as a low-cost alternative to CdTe and $CuIn_{1-X}Ga_XSe_2$ (CIGS) absorbers due to their earth-abundant and nontoxic constituents, tunable band gap, and high absorption coefficient.[1−4] One of the major efficiency limitations of CZTS-based solar cells is the low open-circuit voltage[5,6] (V_{OC}) caused by bulk and interface recombination. Ge incorporation into the kesterite structure forming $Cu_2Zn(Sn_{1-X}Ge_X)S_4$ (CZTGS) is used to tune the electronic properties of CZTS, where Ge occupies Sn sites and suppresses the formation of deep defects to reduce bulk recombination.[7−11] Further, Ge incorporation increases the band gap, which can be exploited to realize band-gap grading within the absorber or to facilitate the application as a top cell in a multijunction solar cell.[12−14]

Among the engineering parameters influencing the CZTGS solar cell performance, the composition and structure of the CZTGS absorber and buffer layer, as well as the interfaces between layers such as the absorber/buffer layer, are crucial. A recent study[15] on CZTGS-based solar cells reported unfavorable alignment of the conduction band minimum (CBM) at the interface of CZTGS and the CdS buffer layer, where CdS has a lower CBM compared to CZTGS. Because the absorber/buffer layer heterojunction characteristics impact the solar cell operation, alternative buffer layers are of major importance for improvement of the CZTGS device performance. The $Zn_{1-X}Sn_XO_Y$ (ZTO) buffer layer is a nontoxic alternative to toxic CdS for CZTS(Se)-,[16−19] Cu_2ZnGeS_4-(CZGS-),[20] and CIGS-based[21] solar cells. Atomic layer deposition (ALD) of ZTO further demonstrates uniform and conformal layer growth and allows for opportunities to tune the ZTO band gap by the adjustment of ALD growth conditions.[22] Further, ultrathin passivation layers formed at the absorber/ZTO interface may help to reduce the interface recombination and can contribute to better device efficiencies.

Although the benefit of ZTO buffer layers on CZTS and CZGS has been shown, comprehensive work on CZTGS/ZTO solar cells is still lacking. Surface treatments of the absorber such as sulfurization, air/N_2 annealing, air exposure, or etching applied before buffer layer deposition may change its chemical and electronic properties and thus device performance.[23−26]

The present work aims at making systematical changes in the bulk and absorber/buffer layer interface properties of CZTGS absorbers with different Ge contents and with CdS or ZTO buffer layers and to understand how this may influence the device performance. First, CZTGS absorbers with [Ge]/([Ge] + [Sn]) (GGT) ratios of 0.2 and 0.4 are fabricated, and

Received: July 29, 2024
Revised: October 1, 2024
Accepted: October 14, 2024
Published: October 24, 2024

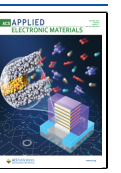

some of the absorbers are exposed to surface treatments including etching and air annealing. Second, experimental conditions during ALD of the ZTO buffer layer, including the deposition temperature (from 100 to 120 °C), film thickness (from 500 to 1000 cycles), and pulse ratio (Zn:Sn = 1:1 and 2:1), are varied, and the resulting CZTGS/ZTO material properties are investigated via synchrotron characterization by X-ray absorption spectroscopy (XAS) and hard X-ray photoelectron spectroscopy (HAXPES). Finally, the related device characteristics, including the current density−voltage ($J-V$) and external quantum efficiency (EQE), are discussed.

EXPERIMENTAL METHODS

CZTGS Fabrication. In this study, a substrate consisting of a molybdenum-coated soda lime glass (SLG) was used. For a better interfacial adhesion between the absorber and substrate[15] and to serve as a diffusion barrier isolating the effects of back-contact chemistry on the electrical properties of the absorber layer,[27] the SLG/Mo substrates were coated with TiN (20 nm) by reactive direct-current (dc) sputtering (Von Ardenne sputtering system) using a Ti target, as described before. The atmosphere was a mixture of Ar:N_2 in the ratio 20:45 at a pressure of 0.8 Pa. The base pressure was below 2×10^{-5} Pa, and deposition was performed without heating the substrate holder.

The CZTGS absorbers with a thickness of about 900 nm and varying Ge content (GGT = 0.2 and 0.4, respectively) were deposited on the SLG/Mo/TiN substrates by cosputtering from copper sulfide (CuS), germanium (Ge), zinc sulfide (ZnS), and tin(II) sulfide (SnS) targets. The sputtering process was performed at a pressure of 0.7 Pa under an Ar atmosphere. The sputter systems used were Kurt J. Lesker for CuS and Ge and a radio-frequency (RF) system with a power density of 3.51 W cm^{-2} for ZnS. The base pressure of the sputter system was maintained below 3×10^{-5} Pa. The concentration of Ge was controlled by varying the applied power to Ge and SnS targets. Throughout the sputter-deposition process, the substrate holder temperature was kept at 250 °C. The composition of the CZTGS precursors was analyzed using X-ray fluorescence (XRF), calibrated using Rutherford back-scattering (RBS). Table 1 summarizes the compositions of the as-deposited CZTGS absorbers as measured by XRF.

Table 1. CZTGS Precursor Compositions Measured with XRF

sample	[Ge]/([Ge] + [Sn])	[Cu]/([Ge] + [Sn])	[Zn]/([Cu] + [Ge] + [Sn])
$CZT_{0.8}G_{0.2}S$	0.22	1.97	0.33
$CZT_{0.6}G_{0.4}S$	0.39	2.02	0.34

CZTGS precursors were annealed and sulfurized after being loaded into a graphite box coated with pyrolytic carbon. We added ∼110 mg of sulfur to the graphite box, which was then placed in a preheated tube furnace. The sulfurization process was carried out under a stable pressure of 450 mbar of Ar. The temperature of the substrate holder increased gradually to 550 °C and dwelled for 13 min, as described elsewhere.[15,28]

After sulfurization, some absorbers underwent further surface treatments by annealing in air (AA) on a hot plate (90 s at 300 °C, followed by 10 min at 200 °C). After the air-annealing treatment, the samples were removed from the hot plate and cooled to room temperature. This surface treatment method was previously shown to be beneficial for CZTS-based absorbers.[29] These samples are labeled as "AA" in Table 2. Prior to buffer layer deposition, most of the absorbers were etched in 5% potassium cyanide (KCN) for 2 min in 1.5 M aqueous solution at room temperature, if not otherwise mentioned in the text.

As a reference buffer layer, CdS was deposited on the CZTGS absorbers by chemical bath deposition (CBD). The CdS films were prepared by mixing thiourea (0.07 M), cadmium acetate (0.005 M), and ammonia (1.14 M) solutions in the bath at a temperature of 60 °C for 8 min and 15 s. The solution was stirred for 10 s each minute. The samples were submerged in a separate beaker of deionized water once CdS deposition was completed. This method produced a nominal thickness of approximately 50 nm CdS on CZTS.[25,29]

The ZTO buffer layers were grown in a Microchemistry F-120 ALD reactor, using nitrogen as a carrier gas. The CZTGS absorbers were loaded into the ALD chamber 30 min prior to ZTO film deposition for temperature stabilization. Diethyl zinc (DEZn) and tetrakis(dimethylamido)tin(IV) (TDMASn) were used as metal sources, while deionized water was used as an oxygen source. The Zn:Sn ratio was changed by adjusting the DEZn-to-TDMASn pulse ratio in the DEZn:TDMASn:N_2:H_2O:N_2 ALD cycle. The thickness of the ZTO layer was changed by varying the number of cycles at a fixed ALD ZTO deposition temperature (T_{ALD}). A total of 1000, 750, and 500 ALD cycles were deposited using 1:1 and 2:1 $ZnO:SnO_2$ supercycle approaches with pulse lengths of 400:800:400:800 ms. The ZTO films were grown at deposition temperatures (T_{ALD}) of 100, 110, and 120 °C. Previous works[17,20,30,31] on similar ZTO ALD conditions showed that the ALD growth temperatures in the range of 100−120 °C, along with ZnO_2:SnO_2 pulse ratios of 1:1 and 2:1, resulted in ZTO films with band gaps in the range of 3.3−3.5 eV, depending on the measurement method. Within each run, a SLG reference piece was used for thickness determination, as described before.[18,32] The XRF-estimated ZTO film thicknesses are ∼15 nm for 500 ALD cycles, ∼30 nm for 500 ALD cycles, and ∼48 nm for 1000 ALD cycles with $ZnO:SnO_2$ = 1:1 and approximately 50 nm for 750 ALD cycles with $ZnO:SnO_2$ = 2:1. Table 2 summarizes the investigated CZTGS samples with CdS and ZTO buffer layers as well as the ZTO properties.

Some of the samples with and without the ALD buffer layer were sealed in a plastic bag under N_2 to avoid contamination and transported to the synchrotron for characterization.

Half (1.25 cm × 2.5 cm) of each sample was later processed into devices by depositing the intrinsic ZnO (i-ZnO) and aluminum zinc oxide (AZO) window layer from i-ZnO and ZnO:Al (2 wt % Al_2O_3 in ZnO) targets by RF and dc sputtering, respectively, in a Von Ardenne sputtering system, as described elsewhere.[33] The solar cells with an area of 0.05 cm^2 were fabricated using mechanical scribing. The completed thin-film solar cells were prepared from stacks consisting of SLG/Mo/TiN/CZTGS/CdS or ZTO/i-ZnO/AZO.

Materials Characterization. The polycrystalline structures of as-prepared CZTGS absorbers were characterized by grazing-incidence X-ray diffraction (GIXRD) in a Siemens D5000 diffractometer, using Cu Kα radiation (wavelength = 1.54 Å), equipped with an X-ray mirror and parallel-plate collimator. A grazing-incidence angle (α) of 1° was used for the measurements, yielding bulk information from within the absorber. The film thicknesses and cross section of CZTGS absorbers were measured using scanning electron microscopy (SEM) in a Zeiss LEO 1550 system equipped with a field-emission gun at a low accelerating voltage (3 kV) to improve the imaging details of morphology.

Synchrotron Characterization. The local environment of Ge atoms in the bulk of CZTGS absorbers with varying Ge content with the buffer layer were probed by XAS measurements. The films in the form of SLG/Mo/TiN/CZTGS/ZTO were measured in fluorescence geometry using a Si-PIN photodiode at Beamline KMC-2 at the BESSY II synchrotron radiation facility in Germany.[34] Linearly polarized X-rays were monochromatized using a Ge-graded Si(111) double-crystal monochromator to measure Ge K-edge XAS at room temperature at a 10° incidence angle, yielding bulk information. Ge foil was measured simultaneously with the samples for energy calibration. The XAS measurements included both the X-ray absorption near-edge structure (XANES) and extended X-ray absorption fine structure (EXAFS) regions. *ATHENA* software, part of the *Demeter* package,[35] was used for preprocessing of the XANES and EXAFS data. Preprocessing of the data included alignment, edge calibration, deglitching, normalization, and background subtraction. A correction model for the self-absorption effect was used in the XAS

https://doi.org/10.1021/acsaelm.4c01317
ACS Appl. Electron. Mater. 2024, 6, 7989−7999

Table 2. Summary of Investigated CZTGS Samples with GGT Ratios of 0.2 and 0.4 Including an Absorber Surface Treatment Description (fresh = Nontreated, AA = Air-Annealed, and KCN = Etched in KCN Solution) and ALD ZTO Conditions [T_{ALD} = ALD Temperature, #ALD cycles = Number of ALD ZTO Cycles, ZnO:SnO_2 Pulse Ratio, and XRF Sn/(Sn + Zn) = RBS-Calibrated XRF][a]

					ALD ZTO conditions			
no.	sample label	GGT ratio	surface treatment on the absorber		T_{ALD} (°C)	#ALD cycles	ZnO:SnO_2 pulse ratio	XRF Sn/(Sn + Zn)
1	0.2-CdS	0.2	fresh	KCN				
2	0.2-120C-1000c		fresh	KCN	120	1000	1:1	0.20
3	0.2-120C-750c		fresh	KCN	120	750	1:1	0.21
4	0.2-120C-750c-2:1		fresh	KCN	120	750	2:1	0.15
5	0.2-120C-500c		fresh	KCN	120	500	1:1	0.21
6	0.2-110C-750c		fresh	KCN	110	750	1:1	0.20
7	0.2-110C-500c		fresh	KCN	110	500	1:1	0.19
8	0.2−100C-750c		fresh	KCN	100	750	1:1	0.19
9	0.2-100C-500c		fresh	KCN	100	500	1:1	0.21
10	0.4-CdS	0.4	fresh	KCN				
11	0.4-CdS-AA		AA	KCN				
12	0.4-120C-1000c		fresh	KCN	120	1000	1:1	0.20
13	0.4-120C-750c		fresh	KCN	120	750	1:1	0.21
14	0.4-120C-750c-2:1		fresh	KCN	120	750	2:1	0.15
15	0.4-120C-500c		fresh	KCN	120	500	1:1	0.21
16	0.4-110C-750c		fresh	KCN	110	750	1:1	0.20
17	0.4-110C-500c		fresh	KCN	110	500	1:1	0.19
18	0.4-110C-500c-AA		AA	KCN	110	500	1:1	0.19
19	0.4-100C-750c		fresh	KCN	100	750	1:1	0.19
20	0.4-100C-500c-Nonetched		fresh	no KCN etch	100	500	1:1	0.21
21	0.4-100C-500c-Nonetched-AA		AA	no KCN etch	100	500	1:1	0.21

[a]GGT = [Ge]/([Ge] + [Sn]); AA = air-annealed. Note that the samples without an "AA" label were fresh (no air-annealing treatment applied) before KCN etching. The CdS thickness is nominal thickness. The difference in band-gap values for ZTO films grown at 120 °C with ZnO:SnO_2 pulse ratios of 1:1 and 2:1 is likely around 0.1 eV, with a maximum variation of up to 0.2 eV.

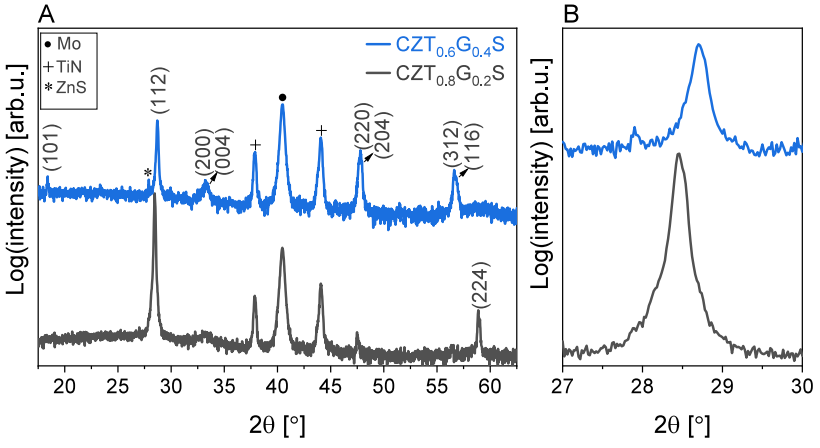

Figure 1. (A) GIXRD (α = 1°) of sulfurized and KCN-etched SLG/Mo/TiN/CZTGS, where the GGT ratios of CZTGS are 0.2 (black, $CZT_{0.8}G_{0.2}S$) and 0.4 (blue, $CZT_{0.6}G_{0.4}S$). The XRD peak positions are consistent with the reference patterns of CZTS,[38] CZGS,[44] Mo,[45] TiN,[41] and ZnS.[40] CZTGS exists as either a kesterite or stannite polymorph (indistinguishable by XRD). Other secondary phases (Cu_2SnS_3 and Cu_2GeS_3) could not be excluded due to overlapping XRD peaks. (B) Peak at 2θ = 28.4° corresponding to the (112) plane shifted due to increased Ge content.

data by using *ATHENA* software.[35] The edge energy at the Ge K-edge was determined by the first inflection point of the corresponding absorption edge data characterizing the reference Ge foil and calibrated to the reported energy (11.1 keV).

The chemical properties of CZTGS/ZTO samples were analyzed by HAXPES measurements performed at Beamline I09 at Diamond Light Source[36] (U.K.). The photoemission measurements were conducted by employing a VG Scienta EW4000 energy electron analyzer at a normal emission. To gain information on the interface between the absorber and buffer layer, CZTGS/ZTO, the photon excitation energy was set to $h\nu$ = 4 keV. A pass energy of 200 eV and an electron analyzer slit width of 0.3 mm (yielding an analyzer resolution of 150 meV) were used. The Fermi edge spectrum of a grounded clean Cu foil was measured for binding energy calibration. The radiation damage was minimized using a defocused beam. *Igor Pro* software was used to fit the XPS line intensities with the Voigt profiles and a linear background.

Device Characterization. The device performance of the investigated solar cells was studied by $J-V$ measurements. The $J-V$ characteristics were determined using a home-built solar simulator

https://doi.org/10.1021/acsaelm.4c01317
ACS Appl. Electron. Mater. 2024, 6, 7989−7999

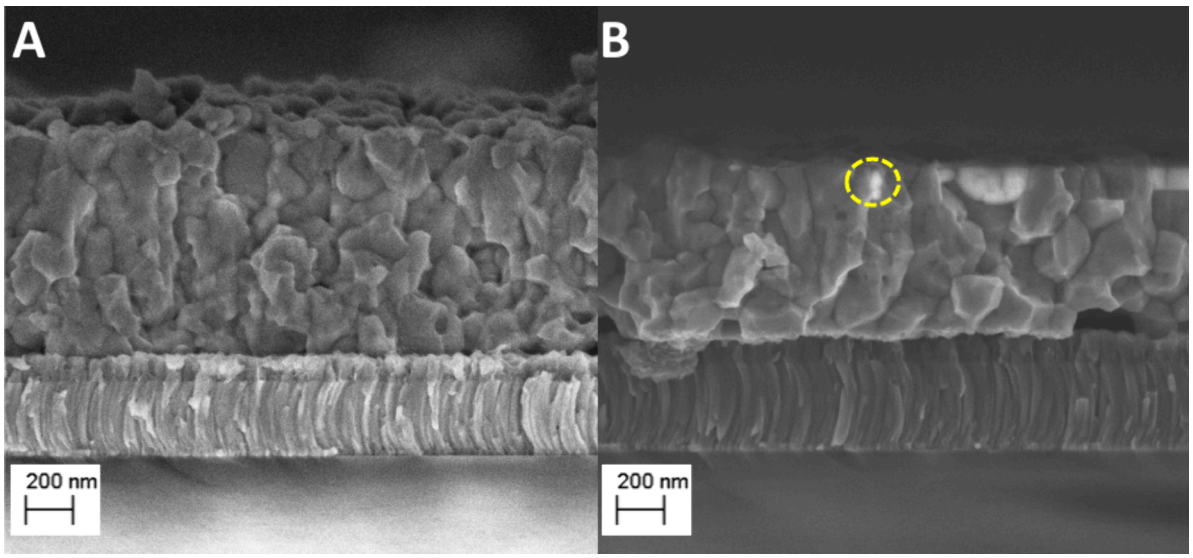

Figure 2. SEM cross-sectional imaging of sulfurized and KCN-etched (A) $CZT_{0.8}G_{0.2}S$ and (B) $CZT_{0.6}G_{0.4}S$ absorbers. The ZnS phase (yellow circle) was observed on the surface of the $CZT_{0.6}G_{0.4}S$ absorber.

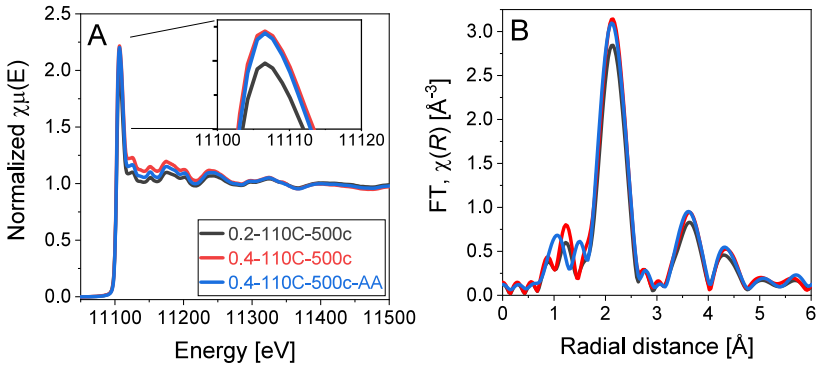

Figure 3. Comparison of (A) normalized XANES spectra and (B) magnitude of the FT (k^2-weighted) EXAFS data at the Ge K-edge for the $CZT_{0.8}G_{0.2}S$ (black, sample 0.2-110C-500c), $CZT_{0.6}G_{0.4}S$ (red, sample 0.4-110C-500c), and $CZT_{0.6}G_{0.4}S$ (blue, sample 0.4-110C-500c-AA) absorbers with ZTO buffer layers deposited at T_{ALD} = 110 °C and number of ALD ZTO cycles = 500. The inset area in part A depicts the intensity change in the normalized XANES. The XAS data were collected at room temperature.

that was calibrated using a Si reference cell. The raw $J-V$ data of all devices are shown in Figure S1. Measurements of the EQE were performed in a homemade EQE system. The system is composed of a xenon glow discharge lamp, a filter wheel, and a chopper with a frequency of 70 Hz. Before the EQE measurements, the system was calibrated using the Hamamatsu Si and InGaAs reference cells. The EQE curves of devices are shown in Figure S2.

RESULTS AND DISCUSSION

Crystal Structures of CZTGS Absorbers. The crystal structures of fabricated absorbers (KCN-etched) were characterized by GIXRD with an α incidence angle of 1°. Figure 1A shows the XRD patterns of the $CZT_{0.8}G_{0.2}S$ and $CZT_{0.6}G_{0.4}S$ samples. The diffraction pattern shows well-defined peaks at 2θ = 18.3°, 28.4°, 33.2°, 47.7°, 56.6°, and 58.8°, which correspond well with the (101), (112), (200), (220), (312), and (224) planes of tetragonal Cu_2ZnSnS_4 and Cu_2ZnGeS_4.[20,37,38] The XRD results indicate that the investigated CZTGS are crystallized in kesterite or stannite phases.[15,39] The data show that the ZnS phase[40] can be present in trace amounts (the peak at 2θ = 27.9° denoted by *) for the 0.4 Ge absorber. The formation of other insulating secondary phases such as $Zn_{0.5}Ge_{0.25}S$, Cu_2SnS_3, or Cu_2GeS_3 or highly conductive phases such as Cu_2S can be present and might be difficult to distinguish due to XRD peak overlap especially for a low Ge amount.[12,39] Figure 1B shows that the XRD peak at 2θ = 28.4° belonging to (112) plane is slightly broader for $CZT_{0.8}G_{0.2}S$ than $CZT_{0.6}G_{0.4}S$. The XRD data further indicate peaks coming from the substrate that belong to Mo at 2θ = 40.4° and from TiN at 2θ = 37.8° and 44.0°.[12,41]

In addition, as the concentration of Ge increases, the lattice parameter of CZTS contracts. This contraction is caused by the relatively smaller size of the Ge atom compared to Sn, leading to a ~0.25° shift of the (112) XRD peak (Figure 1B).[42,43] The observed shift is in good agreement with the results reported by Mora-Herrera et al.[43] and has been observed to be a gradual shift as a function of increasing Ge content from GGT = 0 to 1.0, demonstrating a phase transition from the tetragonal CZTS phase to the orthorhombic CZGS phase.

Morphology of CZTGS Absorbers. The morphology and grain shapes of sulfurized and KCN-etched CZTGS samples with different GGT ratios were characterized by SEM. Figure 2 shows the cross-sectional SEM of the CZTGS samples. Both of the films seem compact and have no cracks, whereas only a few voids are observed. The CZTGS samples show good

https://doi.org/10.1021/acsaelm.4c01317
ACS Appl. Electron. Mater. 2024, 6, 7989−7999

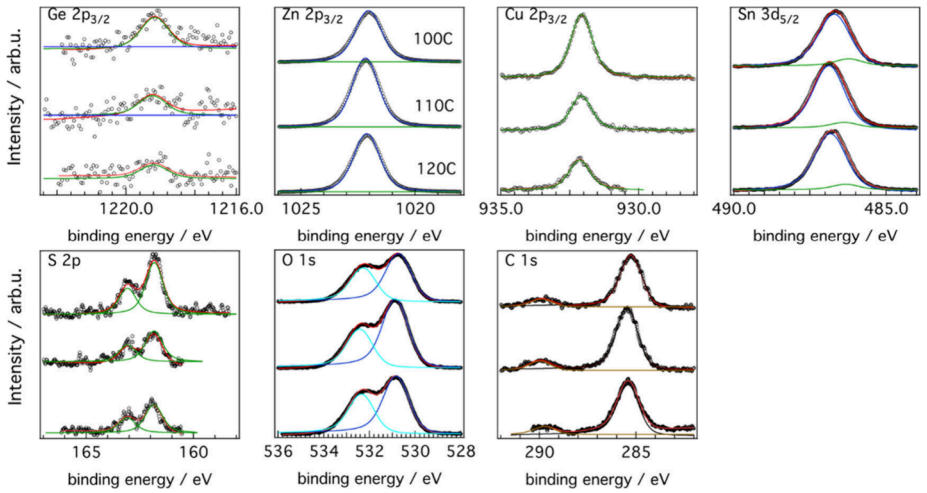

Figure 4. Photoemission spectra (HAXPES) on $CZT_{0.8}G_{0.2}S$ with the ZTO buffer layer deposited at T_{ALD} = 120, 110, and 100 °C and for the number of ALD ZTO cycles of 500 (samples from bottom to top: 0.2-120C-500c, 0.2-110C-500c, and 0.2-100C-500c) recorded with an excitation energy of 4 keV. The spectra include the Ge $2p_{3/2}$, Zn $2p_{3/2}$, Cu $2p_{3/2}$, Sn $3d_{5/2}$, S 2p, O 1s, and C 1s core levels as indicated.

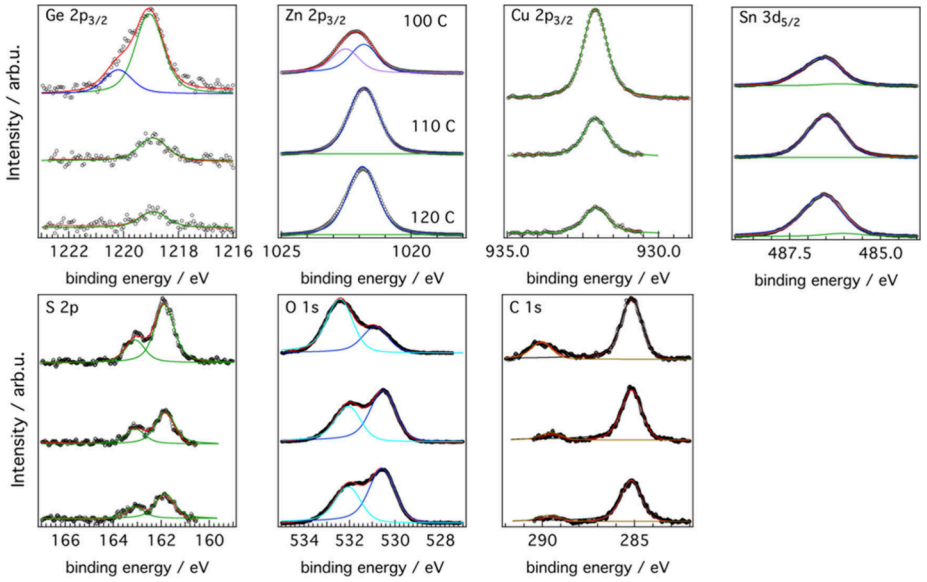

Figure 5. Photoemission spectra (HAXPES) on $CZT_{0.6}G_{0.4}S$ with the ZTO buffer layer deposited at T_{ALD} = 120, 110, and 100 °C and for the number of ALD ZTO cycles of 500 (samples from bottom to top: 0.4-120C-500c, 0.4-110C-500c, and 0.4-100C-500c-Nonetched) recorded with an excitation energy of 4 keV. The spectra include the Ge $2p_{3/2}$, Zn $2p_{3/2}$, Cu $2p_{3/2}$, Sn $3d_{5/2}$, S 2p, O 1s, and C 1s core levels as indicated.

adherence to the substrate, due to the TiN interlayer between Mo and CZTGS that improves adhesion markedly.[15] A comparison of the CZTGS absorbers with varying Ge content shows that the crystallization and grain size are similar for $CZT_{0.8}G_{0.2}S$ and $CZT_{0.6}G_{0.4}S$ absorbers. The film thicknesses determined by the SEM cross section are 900 ± 50 and 870 ± 40 nm for $CZT_{0.8}G_{0.2}S$ and $CZT_{0.6}G_{0.4}S$ absorbers, respectively. This difference may possibly be due to material loss, such as GeS, during sulfurization at high temperature, as previous studies also reported.[39,42]

In addition to the voids in the higher-Ge-content CZTGS absorber (Figure 2), secondary phases are investigated for the cross-sectional morphology of the film. The appearance of the insulating ZnS phase[12] is visible (highlighted by the yellow circle) on the surface of $CZT_{0.6}G_{0.4}S$. Because only a limited surface area of each sample was investigated, we cannot exclude the presence of secondary phases on the 0.2 Ge sample. Further, the formation of other phases, such as GeO_X, is not observed within the investigated areas.

Bulk Properties of CZTGS/ZTO Studied by XAS. To understand the bulk properties of CZTGS/ZTO samples with different Ge contents, XAS data containing both XANES and EXAFS regions were collected at the Ge K-edge at room temperature (Figure 3). XANES provides high sensitivity to changes in the electronic structures and formal metal oxidation states of the element, while EXAFS spectroscopy provides evidence of the structure around an absorbing atom, identification of ligands, and bond distances.[46] The measurements were performed on two representative $CZT_{0.8}G_{0.2}S$ and $CZT_{0.6}G_{0.4}S$ absorbers with ZTO buffer layers (T_{ALD} = 110 °C; 500 ALD cycles). In Figure 3A, a comparison of the normalized XANES spectra of the two CZTGS/ZTO samples demonstrates an increasing XANES intensity with increasing Ge content in the absorber from GGT = 0.2 to 0.4, as expected. The lack of shift in the edge position in the spectra

https://doi.org/10.1021/acsaelm.4c01317
ACS Appl. Electron. Mater. 2024, 6, 7989−7999

indicates that the chemical states of Ge atoms in the two samples are similar.[47] The magnitudes of the Fourier-transformed (FT) Ge K-edge EXAFS spectra of the same samples are presented in Figure 3B, where the radial distance indicates the distance to the neighboring atoms from the absorbing atom (Ge). In the CZTGS structure, the nearest neighboring atoms to each Ge atom is S.[37] Thereby, in the FT of the EXAFS data, the feature at ∼2.15 Å represents mostly phase-shift uncorrected Ge−S bonds,[48] typically underestimated by ∼0.3−0.4 Å from the ideal bulk Ge−S bond length. The shapes of the FT of the EXAFS spectra of CZTGS/ZTO samples with varying Ge content are similar to each other (Figure 3B). Therefore, the local environment around the Ge atoms within the CZTGS absorber on a subnanometer scale is not notably affected by the Ge content of the CZTGS/ZTO samples, and only an increased relative concentration of Ge−S bonds is observed in the EXAFS FT data, as expected for the higher Ge content absorber.

Figure 3 also shows the Ge K-edge XAS data collected on $CZT_{0.6}G_{0.4}S$/ZTO that had a postdeposition air-annealing absorber surface treatment (red curve). The XANES and FT of the EXAFS of CZTGS/ZTO with and without absorber surface air annealing are very similar, indicating that the bulk local environment of Ge atoms do not change significantly due to air annealing. A discussion on the correlation between the bulk properties (in terms of increased Ge content and surface treatments) and the solar cell device performance of these samples is made in the following sections.

Chemical Properties of the CZTGS/ZTO Interface Studied by HAXPES. To investigate the near-interface region between the CZTGS absorbers with different Ge contents and the ZTO buffer layers, HAXPES measurements were performed by employing an excitation energy of 4 keV, corresponding to an average probing depth of 17 nm. Figures 4 and 5 show a comparison of the HAXPES data of $CZT_{0.6}G_{0.4}S$/ZTO and $CZT_{0.8}G_{0.2}S$/ZTO interfaces with the ZTO buffer layer (500 ALD ZTO cycles) deposited at T_{ALD} = 100, 110, and 120 °C. Similar to our recent study on CZGS/ZTO,[49] the results in Figures 4 and 5 show that, for both CZTGS/ZTO sample series, mostly metal sulfide species from the CZTGS kesterite are observed for the absorber signals (single peaks in Ge $2p_{3/2}$ and Cu $2p_{3/2}$ and a doublet in S 2p), in addition to the metal oxides observed from the ZTO buffer (green components in Zn $2p_{3/2}$, Sn $3d_{5/2}$, and O 1s). Carbon contamination at ∼285 eV and some weak carbonate species at ∼289 eV are also observed on all samples, likely due to air exposure of both the absorber or absorber/buffer surfaces.

Some weak Sn−S and Zn−S components (blue) from the CZTGS kesterite are observed at the employed photon energy, which are more visible for the lower Ge content absorber (0.2 Ge) due to the increased presence of Sn and Zn at the surface of CZTGS. In Figure 5, the high-binding-energy component (purple) observed for the Zn 2p core levels from the nonetched sample (sample 0.4-100C-500c-Nonetched) is not fully understood, but because an increased intensity of hydroxide species (light blue component) is observed in O 1s, we assume that they may be related to hydroxide species.

For the KCN-etched absorber samples, only the Ge−S component from CZGTS is observed in the Ge 2p core level (Figures 4 and 5). The Ge 2p spectrum of the non-KCN-etched sample further shows the presence of germanium oxide (blue component) in addition to Ge−S from CZTGS kesterite (green component) (Figure 5). The observed germanium oxide is likely GeO_2, which is consistent with the previous reports on CZGS-[12] and CZTGSe-based[50] solar cells, where GeO_2 has been observed both within the absorber and at the grain boundaries. These findings align with our recent observation of GeO_2 at the CZGS/ZTO interface for nonetched absorber,[49] attributed to the diffusion and accumulation of germanium toward the absorber surface. For this sample, the results further show an increase in the intensity of the high-binding-energy component in O 1s, which is likely due to an increase in the hydroxide (−OH) species on the surface of the absorber, as previously observed for the CZTS absorber.[29] Thus, the results indicate that GeO_2 forms at the surface of CZTGS during fabrication, presumably during the cooling process after sulfurization or during air exposure before ZTO deposition,[49] and is preserved upon ALD buffer layer growth if no chemical etch treatment is applied before the buffer layer growth. The samples that could not be etched before buffer layer deposition (due to delamination issues) would thus have the GeO_2 species preserved after buffer layer deposition.

Solar Cell Device Behavior. *J−V Characteristics.* Table 3 presents the device performance (*J−V* characteristics) of the investigated CZTGS samples with GGT ratios of 0.2 and 0.4. Device performance parameters include power conversion efficiency (PCE, η), short-circuit current density (J_{SC}), fill factor (FF), and open-circuit voltage (V_{OC}).

Table 3. *J−V* Characteristics (Best Cell Results) of the Investigated $CZT_{0.8}G_{0.2}S$ and $CZT_{0.6}G_{0.4}S$ Devices[a]

		device performance			
no.	sample label	η (%)	V_{OC} (mV)	J_{SC} (mA cm^{-2})	FF (%)
1	0.2-CdS	1.0	406	5.3	46.0
2	0.2-120C-1000c	1.5	481	7.1	43.8
3	0.2-120C-750c	2.6	646	7.4	53.9
4	0.2-120C-750c-2:1	0.77	354	5.8	37.6
5	0.2-120C-500c	1.99	576	8.1	42.7
6	0.2-110C-750c	1.31	565	6.9	36.9
7	0.2-110C-500c	2.06	612	7.1	47.2
8	0.2-100C-750c	1.17	643	6.6	27.4
9	0.2-100C-500c	0.14	96	5.9	25.2
10	0.4-CdS	1.42	577	5.2	47.1
11	0.4-CdS-AA	1.12	561	3.3	59.9
12	0.4-120C-1000c	2.8	706	6.4	62.2
13	0.4-120C-750c	2.65	708	6.4	58.7
14	0.4-120C-750c-2:1	2.31	656	5.9	61.2
15	0.4-120C-500c	2.5	698	7.1	50.2
16	0.4-110C-750c	2.34	668	5.7	61.9
17	0.4-110C-500c	2.45	662	6.2	59.3
18	0.4-110C-500c-AA	2.73	768	5.9	60.5
19	0.4-100C-750c	delamination			
20	0.4-100C-500c-Nonetched	1.27	708	5.9	30.4
21	0.4-100C-500c-Nonetched-AA	1.37	653	4.1	51.6

[a]V_{OC} = open-circuit voltage, J_{SC} = short-circuit current density, FF = fill factor, and η = power conversion efficiency. The raw *J−V* data of all devices are shown in Figure S1.

The *J−V* parameters in Table 3 demonstrate that the highest PCE (2.8%) and FF (62.2%) values are obtained for the CZTGS/ZTO devices when a thick ZTO (1000 ALD cycles) is deposited on the higher-Ge-content (GGT = 0.4) absorber,

https://doi.org/10.1021/acsaelm.4c01317
ACS Appl. Electron. Mater. 2024, 6, 7989−7999

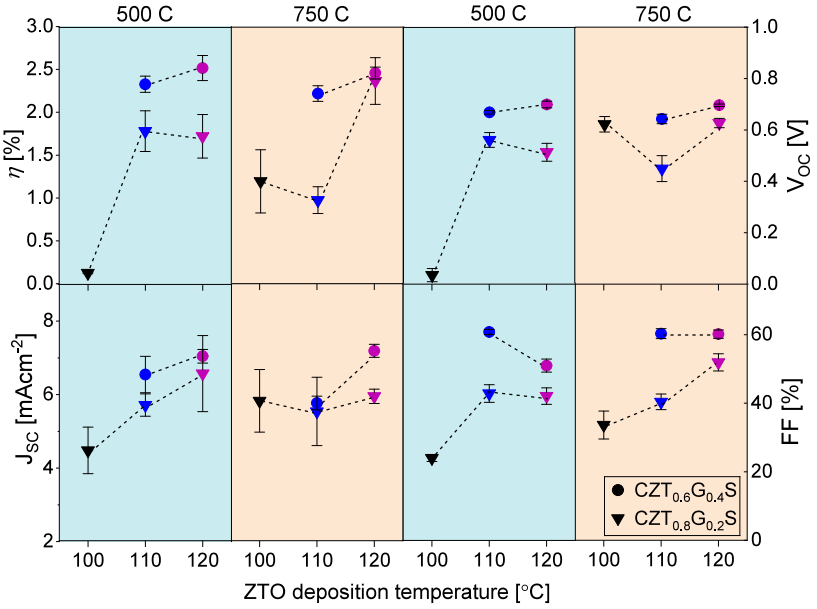

Figure 6. Solar cell parameters of $CZT_{0.8}G_{0.2}S$ (triangle symbols) and $CZT_{0.6}G_{0.4}S$ (circle symbols) solar cells with ZTO buffer layers employing different ALD ZTO deposition conditions. The number of ALD ZTO deposition cycles were 500 (blue area) and 750 (orange area), and the ZTO T_{ALD} are 100 °C (black symbols), 110 °C (blue symbols), and 120 °C (purple symbols). The solar cell parameters, along with their deviations, are provided for each sample, with an average of 10 cells per sample.

$CZT_{0.6}G_{0.4}S$, at T_{ALD} = 120 °C and with $ZnO:SnO_2$ = 1:1 pulse ratio (sample 0.4-120C-1000c). The highest V_{OC} (768 mV) is observed on the air-annealed $CZT_{0.6}G_{0.4}S$ solar cells with a ZTO buffer layer deposited at T_{ALD} = 110 °C for 500 cycles (sample 0.4-110C-500c-AA), while the highest J_{SC} (8.1 mA cm^{-2}) is observed on the lower-Ge-content $CZT_{0.8}G_{0.2}S$ absorber at T_{ALD} = 120 °C for 500 cycles (sample 0.2-120C-500c). No device could be fabricated for sample 0.4-100C-750c due to complete delamination, and that sample is thus excluded. The $J-V$ data of all samples are given in Figure S1.

Below we investigate the effects of the buffer layer type and properties, absorber Ge content, and surface treatments on the solar cell performance of CZTGS devices.

Influence of CdS and ZTO Buffer Layers on the Device Performance. From the $J-V$ characteristics presented in Table 3, the benefit of ZTO on the conversion efficiency is shown. Overall, $CZT_{0.8}G_{0.2}S$ devices demonstrate better PCE values with a ZTO buffer layer than with a CdS buffer layer. For the $CZT_{0.6}G_{0.4}S$ absorbers, the PCE values of CZTGS solar cells with the ZTO buffer layer (between 2.3 and 2.8%) are always higher than that with the CdS buffer layer (1.42%).

A comparison of the FF values of $CZT_{0.8}G_{0.2}S$ absorbers with ZTO and CdS buffer layers shows that the FF is reduced with ZTO buffers, except for the device with a ZTO buffer deposited at T_{ALD} = 120 °C with a Zn:Sn pulse ratio of 1:1 for 750 ALD ZTO cycles (Table 3). In contrast, all of the higher-Ge-content devices with $CZT_{0.6}G_{0.4}S$ absorbers show higher FF values with ZTO as compared to CdS buffer.

The J_{SC} values for $CZT_{0.8}G_{0.2}S$ absorbers with CdS and ZTO buffers vary but are higher on $CZT_{0.6}G_{0.4}S$ absorbers with the CdS buffer layer than with ZTO. We note that the thicknesses of the buffer layers are different (between 15 and 50 nm ZTO layers versus 50 nm CdS layer, as indicated in Table 1); thus, a direct J_{SC} comparison may not be accurate.

The average V_{OC} is significantly increased when the ZTO buffer layer is used on both the $CZT_{0.8}G_{0.2}S$ (up to 646 mV) and $CZT_{0.6}G_{0.4}S$ (up to 768 mV) absorbers. The significant V_{OC} improvement in this study might be due to a better band alignment between CZTGS and the high-band-gap ZTO compared to CdS.[31,51,52] Similar results have previously been obtained on CZTS-based devices.[17]

Influence of Increased Ge Content on the Device Performance. In Table 3 and Figure 6, the solar cell parameters characterizing the devices with 500 and 750 ALD cycles show that the PCE values of solar cell devices with a GGT ratio of 0.4 are higher than those of samples with a GGT ratio of 0.2, regardless of T_{ALD}. We also find that the V_{OC}, J_{SC}, and FF values of the devices increase with increasing Ge content. Thus, a higher absorber band gap due to increased Ge content may explain the observed increased device efficiency to some extent.

A similar behavior has been observed for the $CZT_{0.8}G_{0.2}S$/ZTO devices with 1000 ALD cycles and T_{ALD} of 120 °C (samples 0.2-120C-1000c versus 0.4-120C-1000c; Table 3). The higher efficiencies of $CZT_{0.6}G_{0.4}S$/ZTO than of $CZT_{0.8}G_{0.2}S$/ZTO devices are likely attributed to the improved J_{SC} and FF, consistent with the results of other works.[7] Although small increases in GGT from 0.2 to 0.4 result in an improved device performance in this work, a significant increase in the Ge content usually leads to a PCE drop due to deep defects or secondary phases.[7,53,54] Previous research on $Cu_2Zn(Sn,Ge)(S,Se)_4$/CdS devices showed that increasing the Ge content up to GGT = 0.25 increases the absorber band gap as well as the overall efficiency up to 11%, whereas beyond GGT = 0.5, the device efficiency decreases rapidly. In addition, in the works of Saini et al.,[15,20] a record-high V_{OC} value (1.1 V) for a fully germanized Cu_2ZnGeS_4/ZTO device was observed, while the PCE was low (0.86%) due to existence of GeO_2 species[28] at the interface, which contributed to current blocking, resulting in a low FF (38%). In this work, the possibility of applying a KCN-etch treatment helps to remove those secondary phases; therefore, the device performance is not negatively influenced by them. Further, a better band alignment between the ZTO buffer and higher-band-gap

https://doi.org/10.1021/acsaelm.4c01317
ACS Appl. Electron. Mater. 2024, 6, 7989−7999

absorber (higher Ge content) may also contribute to improved device performance.

Influence of ALD ZTO Conditions on the Device Performance. 1. ALD ZTO Temperature. In Figure 6, the solar cell parameters of CZTGS/ZTO devices fabricated from KCN-etched absorbers as a function of the ALD ZTO process temperature are given for 500 and 750 ALD cycles. Each parameter is presented as the average of 10 solar cells from a device, along with their standard deviations. For the $CZT_{0.8}G_{0.2}S$/ZTO devices with 500 ALD ZTO cycles, an increase in T_{ALD} from 100 to 110 °C results in an improved solar cell performance with increased PCE, V_{OC}, J_{SC}, and FF. As T_{ALD} increases from 110 to 120 °C, there is only a slight change in the device performance (Figure 6 and Table 3). The solar cell parameters for the higher-Ge-containing devices, $CZT_{0.6}G_{0.4}S$/ZTO, with increasing T_{ALD} demonstrate a very similar trend, except for a relatively flat V_{OC} value throughout all T_{ALD} for 500 ALD cycles. The small variation in the device performance with the ALD ZTO temperature indicates that the chemical properties at the CZTGS/ZTO interface are similar, also confirmed by the HAXPES results presented earlier, which show similar results for the etched samples. These small changes are consistent with the results of other works[20,49] from our group on CZGS devices that demonstrate only a small variation in the ZTO band gap for the ALD temperature change from 110 to 120 °C (0.1 eV) and also no significant changes in the device performance with the ALD temperature change, suggesting similar interface properties. In that previous work,[20] non-KCN-etched CZGS/ZTO devices fabricated at the same ZTO deposition conditions (T_{ALD} = 120 °C, #ALD cycles = 750) show a very high V_{OC} (989 mV) and low PCE, FF, and J_{SC} values (Table 3).

For the CZTGS absorbers with 750 ALD ZTO cycles, increased PCE, J_{SC}, and FF values are observed with increasing T_{ALD} from 100 to 110 and to 120 °C, while V_{OC} values remain nearly unchanged. It is important to mention that the deviations for $CZT_{0.8}G_{0.2}S$ devices with 750 ALD ZTO deposition cycles at a T_{ALD} of 100 °C are high, which may influence the observed trends.

2. Number of ALD ZTO Cycles/Thickness. In Table 3 and Figure 6, the $J-V$ parameters characterizing $CZT_{0.6}G_{0.4}S$/ZTO demonstrate that, at T_{ALD} = 120 °C, the PCE, V_{OC}, and FF values of devices do not change significantly with the number of ALD ZTO cycles, whereas J_{SC} increases with decreasing ALD ZTO cycles from 1000 to 500. All device performance parameters collected on $CZT_{0.6}G_{0.4}S$/ZTO at T_{ALD} = 110 °C are relatively flat (Figure 6). Due to delamination issues of the films at T_{ALD} = 100 °C, we lack data for comparison.

For the device performance of $CZT_{0.8}G_{0.2}S$/ZTO, the highest PCE (2.6%), V_{OC} (646 mV), and FF (53.9%) values at T_{ALD} = 120 °C are obtained for 750 ALD ZTO cycles. The other samples (ALD ZTO cycles of 1000 and 500) do not present any reasonable correlations with the device performance. For these devices, improved $J-V$ characteristics have been observed at T_{ALD} = 110 °C when the number of cycles decrease from 750 to 500 (Table 3). Yet, at T_{ALD} = 100 °C, the device performance is lower for samples with 500 ALD cycles than with 750 ALD cycles. A reason for this behavior may be a very thin buffer layer that could have been sputtered through during window layer deposition.

3. Zn:Sn Pulse Ratio in ALD ZTO Deposition. ZTO buffers with varying Zn:Sn pulse ratios (1:1 and 2:1) were investigated as described in the Experimental Methods section. As shown in Table 3, for ZTO deposition at T_{ALD} = 120 °C and for 750 ALD cycles, the $CZT_{0.8}G_{0.2}S$/ZTO device with Zn:Sn = 1:1 outperforms the device with ALD ZTO deposited with Zn:Sn = 2:1 in terms of all $J-V$ characteristics. The overall efficiency of the former one is 2.66%, whereas the latter one has a PCE of only 0.77%. This finding is consistent with other studies[32] on CIGS/ZTO solar cells, where both V_{OC} and the FF increase with increased Sn content up until a Zn:Sn pulse ratio of 3:8. Some earlier work[22,55−57] showed the dependence of the ZTO band gap on the Zn:Sn pulse ratio grown at different temperatures and with different ALD ZTO cycles that could be linked to the changing device performance. For instance, a CIGS/ZTO[55] device with ZTO deposition at T_{ALD} of 120 °C shows that changing the Zn:Sn pulse ratio from 9:1 to 4:1 increases the ZTO band gap from 2.2 to 3.0 eV, while a more significant change in the Zn:Sn pulse ratio results in a lower band gap.

The devices with higher Ge content, $CZT_{0.6}G_{0.4}S$/ZTO, show a similar tendency, yet the dependence of the device efficiency and FF on the Zn:Sn pulse ratio of ALD ZTO is not as substantial (only ∼0.3 and 3% change, respectively) because only a small variation in the Zn:Sn pulse ratio was tested in this study. On the other hand, a larger decrease is observed in V_{OC} from 708 to 656 mV with increased Zn:Sn pulse ratio. We may thus conclude that a better band alignment is obtained between CZTGS and ZTO with a Zn:Sn pulse ratio of 1:1.

Influence of the Absorber Surface Treatments on the Device Performance. One of the surface treatments of the kesterite absorbers that previously have shown increased device performance is air annealing, which may affect the chemical and electronic properties of absorbers and the subsequent deposition of different buffer layers.[18,29] Prior studies have proposed various outcomes resulting from the air annealing of CZTS, such as the passivation of grain boundaries,[58] modification of surface composition, or even band-gap widening.[17] In this work, we investigated the influence of air annealing of the $CZT_{0.6}G_{0.4}S$ absorber surface on the device performance of solar cells. In Table 3, a comparison of the solar cell parameters of fresh (0.4-110C-500c) and air-annealed (0.4-110C-500c-AA) $CZT_{0.6}G_{0.4}S$/ZTO devices indicates that, with air annealing, the PCE and V_{OC} of the devices improve, while the J_{SC} and FF values do not show a notable change. Further, the PCE decreases for the nonetched absorber samples, similar to previous results on CZGS/ZTO,[20] and is likely due to the presence of GeO_2 species at the buffer/absorber heterojunction. A decrease in V_{OC} is observed for the device obtained by air annealing the $CZT_{0.6}G_{0.4}S$ absorber without KCN etching (samples 0.4-100C-500c-Nonetched versus 0.4-100C-500c-Nonetched-AA). The CZTGS absorbers with CdS buffer layers show an unusual device performance behavior with air annealing, where V_{OC} remains the same and J_{SC} drops significantly, which would indicate current blocking.

CONCLUSIONS

CZTGS solar cells with varying Ge content and with CdS and ZTO buffer layers are fabricated successfully and structurally characterized by SEM and XRD. Using synchrotron XAS and HAXPES measurements, the bulk and absorber/buffer interface properties of CZTGS are studied. The property−performance relationship of the solar cells is investigated based on the Ge content, variations in the ALD ZTO deposition conditions, and the absorber surface treatments.

https://doi.org/10.1021/acsaelm.4c01317
ACS Appl. Electron. Mater. 2024, 6, 7989−7999

The results indicate some dependence of the solar cell performance with the buffer layer type and properties, as well as the absorber Ge content and surface treatments. Overall, a better device performance is observed for a ZTO buffer layer compared to CdS, for CZTGS absorbers with varying Ge content, likely due to a better band alignment at the buffer/absorber interface. It is also observed that the ZTO properties influence the CZTGS/ZTO device performance: the efficiency increases for a thicker ZTO buffer layer and a Zn:Sn pulse ratio of 1:1. An air-annealing treatment of CZTGS improves the performance of KCN-etched "cleaned" devices, and the presence of secondary phases (GeO_2) at the absorber/buffer interface is confirmed for nonetched absorber samples, as previously reported for CZGS devices.

■ ASSOCIATED CONTENT

Supporting Information

The Supporting Information is available free of charge at https://pubs.acs.org/doi/10.1021/acsaelm.4c01317.

J−*V* data of thin-film solar cells and EQE characteristics of devices (PDF)

■ AUTHOR INFORMATION

Corresponding Authors

Melike Babucci − *Solar Cell Technology, Department of Materials Science and Engineering, Uppsala University, Uppsala 75121, Sweden;* orcid.org/0000-0001-7785-3755; Email: melike.babucci@angstrom.uu.se

Natalia M. Martin − *Solar Cell Technology, Department of Materials Science and Engineering, Uppsala University, Uppsala 75121, Sweden;* orcid.org/0000-0002-6881-4989; Email: natalia.martin@angstrom.uu.se

Authors

Tobias Törndahl − *Solar Cell Technology, Department of Materials Science and Engineering, Uppsala University, Uppsala 75121, Sweden;* orcid.org/0000-0001-7757-5847

Soham Mukherjee − *Condensed Matter Physics of Energy Materials, Division of X-ray Photon Science, Department of Physics and Astronomy, Uppsala University, Uppsala 75120, Sweden*

Charlotte Platzer Björkman − *Solar Cell Technology, Department of Materials Science and Engineering, Uppsala University, Uppsala 75121, Sweden*

Complete contact information is available at: https://pubs.acs.org/10.1021/acsaelm.4c01317

Notes

The authors declare no competing financial interest.

■ ACKNOWLEDGMENTS

This work was financially supported by the Swedish Energy Agency (Grants 48 479-1 and P50626-1), the Swedish Research Council (Grants 2020-04065, 2018-06465, 2018-04330, and 2023-05072), and the StandUp for Energy programme. Funding from the European Union's H2020 research and innovation programme under Grant Agreement 952982 (CUSTOM-ART) is acknowledged. This work was carried out with the support of Diamond Light Source, Beamline I09 (Proposal SI30315-1). Support from Dr. Pardeep Thakur Kumar and Dr. Tien-Lin Lee at the Beamline I09 is acknowledged. We acknowledge the use of Beamline KMC-2 at BESSY II.

■ REFERENCES

(1) Platzer Björkman, C.; Larsen, J. K.; Saini, N.; Babucci, M.; Martin, N. Ultrathin Wide Band Gap Kesterites. *Faraday Discuss.* **2022**, *239*, 38.

(2) Keller, J.; Kiselman, K.; Donzel-Gargand, O.; Martin, N. M.; Babucci, M.; Lundberg, O.; Wallin, E.; Stolt, L.; Edoff, M. High-Concentration Silver Alloying and Steep Back-Contact Gallium Grading Enabling Copper Indium Gallium Selenide Solar Cell with 23.6% Efficiency. *Nat. Energy* **2024**, *9*, 467.

(3) Yan, C.; Huang, J.; Sun, K.; Johnston, S.; Zhang, Y.; Sun, H.; Pu, A.; He, M.; Liu, F.; Eder, K.; Yang, L.; Cairney, J. M.; Ekins-Daukes, N. J.; Hameiri, Z.; Stride, J. A.; Chen, S.; Green, M. A.; Hao, X. Cu_2ZnSnS_4 Solar Cells with over 10% Power Conversion Efficiency Enabled by Heterojunction Heat Treatment. *Nat. Energy* **2018**, *3*, 764.

(4) Zhao, Y.; Yuan, S.; Kou, D.; Zhou, Z.; Wang, X.; Xiao, H.; Deng, Y.; Cui, C.; Chang, Q.; Wu, S. High Efficiency CIGS Solar Cells by Bulk Defect Passivation through Ag Substituting Strategy. *ACS Appl. Mater. Interfaces* **2020**, *12*, 12717.

(5) Nakazawa, K. I. Electrical and Optical Properties of Stannite-Type Quaternary Semiconductor Thin Films. *Jpn. J. Appl. Phys.* **1988**, *27*, 2094.

(6) Giraldo, S.; Jehl, Z.; Placidi, M.; Izquierdo-Roca, V.; Perez-Rodriguez, A.; Saucedo, E. Progress and Perspectives of Thin Film Kesterite Photovoltaic Technology: A Critical Review. *Adv. Mater.* **2019**, *31*, No. 1806692.

(7) Collord, A. D.; Hillhouse, H. W. Germanium Alloyed Kesterite Solar Cells with Low Voltage Deficits. *Chem. Mater.* **2016**, *28* (7), 2067.

(8) Collord, A. D.; Hillhouse, H. W. Composition Control and Formation Pathway of CZTS and CZTGS Nanocrystal Inks for Kesterite Solar Cells. *Chem. Mater.* **2015**, *27*, 1855.

(9) Choubrac, L.; Bär, M.; Kozina, X.; Félix, R.; Wilks, R. G.; Brammertz, G.; Levcenko, S.; Arzel, L.; Barreau, N.; Harel, S.; Meuris, M.; Vermang, B. Sn Substitution by Ge: Strategies to Overcome the Open-Circuit Voltage Deficit of Kesterite Solar Cells. *ACS Appl. Energy Mater.* **2020**, *3*, 5830.

(10) Neuschitzer, M.; Rodriguez, M. E.; Guc, M.; Marquez, J. A.; Giraldo, S.; Forbes, I.; Perez-Rodriguez, A.; Saucedo, E. Revealing the Beneficial Effects of Ge Doping on $Cu_2ZnSnSe_4$ Thin Film Solar Cells. *J. Mater. Chem. A* **2018**, *6*, 11759.

(11) Kim, I.; Kim, K.; Oh, Y.; Woo, K.; Cao, G.; Jeong, S.; Moon, J. Bandgap-Graded $Cu_2Zn(Sn_{1-x}Ge_x)S_4$ Thin-Film Solar Cells Derived from Metal Chalcogenide Complex Ligand Capped Nanocrystals. *Chem. Mater.* **2014**, *26*, 3957.

(12) Saini, N.; Larsen, J. K.; Sopiha, K. V.; Keller, J.; Ross, N.; Platzer-Björkman, C. Germanium Incorporation in Cu_2ZnSnS_4 and Formation of a Sn−Ge Gradient. *Phys. Status Solidi (a)* **2019**, *216*, No. 1900492.

(13) Ford, G. M.; Guo, Q.; Agrawal, R.; Hillhouse, H. W. Earth Abundant Element $Cu_2Zn(Sn_{1-x}Ge_x)S_4$ Nanocrystals for Tunable Band Gap Solar Cells: 6.8% Efficient Device Fabrication. *Chem. Mater.* **2011**, *23*, 2626.

(14) Guo, Q.; Ford, G. M.; Yang, W.-C.; Hages, C. J.; Hillhouse, H. W.; Agrawal, R. Enhancing the Performance of CZTSSe Solar Cells with Ge Alloying. *Sol. Energy Mater. Sol. Cells* **2012**, *105*, 132.

(15) Saini, N.; Larsen, J. K.; Lindgren, K.; Fazi, A.; Platzer-Björkman, C. Bandgap Engineered $Cu_2ZnGe_xSn_{1-x}S_4$ Solar Cells Using an Adhesive TiN Back Contact Layer. *J. Alloys Compd.* **2021**, *880*, No. 160478.

(16) Li, X.; Su, Z.; Venkataraj, S.; Batabyal, S. K.; Wong, L. H. 8.6% Efficiency CZTSSe Solar Cell with Atomic Layer Deposited Zn-Sn-O Buffer Layer. *Sol. Energy Mater. Sol. Cells* **2016**, *157*, 101.

(17) Larsen, J. K.; Larsson, F.; Törndahl, T.; Saini, N.; Riekehr, L.; Ren, Y.; Biswal, A.; Hauschild, D.; Weinhardt, L.; Heske, C.; Platzer-

Björkman, C. Cadmium Free Cu_2ZnSnS_4 Solar Cells with 9.7% Efficiency. *Adv. Energy Mater.* **2019**, *9*, No. 1900439.
(18) Martin, N. M.; Törndahl, T.; Babucci, M.; Larsson, F.; Simonov, K.; Gajdek, D.; Merte, L. R.; Rensmo, H.; Platzer-Björkman, C. Atomic Layer Grown Zinc−Tin Oxide as an Alternative Buffer Layer for Cu_2ZnSnS_4-Based Thin Film Solar Cells: Influence of Absorber Surface Treatment on Buffer Layer Growth. *ACS Appl. Energy Mater.* **2022**, *5*, 13971.
(19) Grenet, L.; Emieux, F.; Andrade-Arvizu, J.; De Vito, E.; Lorin, G.; Sánchez, Y.; Saucedo, E.; Roux, F. Sputtered ZnSnO Buffer Layers for Kesterite Solar Cells. *ACS Appl. Energy Mater.* **2020**, *3*, 1883.
(20) Saini, N.; Martin, N. M.; Larsen, J. K.; Hultqvist, A.; Törndahl, T.; Platzer-Björkman, C. Record 1.1 V Open-Circuit Voltage for Cu_2ZnGeS_4-Based Thin-Film Solar Cells Using Atomic Layer Deposition $Zn_{1-x}Sn_xO_y$ Buffer Layers. *Solar RRL* **2022**, *6*, No. 2100837.
(21) Hultqvist, A.; Platzer-Björkman, C.; Zimmermann, U.; Edoff, M.; Törndahl, T. Growth Kinetics, Properties, Performance, and Stability of Atomic Layer Deposition Zn−Sn−O Buffer Layers for $Cu(In,Ga)Se_2$ Solar Cells. *Photovolt. Res. Appl.* **2012**, *20*, 883.
(22) Lindahl, J.; Keller, J.; Donzel-Gargand, O.; Szaniawski, P.; Edoff, M.; Törndahl, T. Deposition Temperature Induced Conduction Band Changes in Zinc Tin Oxide Buffer Layers for $Cu(In,Ga)Se_2$ Solar Cells. *Sol. Energy Mater. Sol. Cells* **2016**, *144*, 684.
(23) Benhaddou, N.; Aazou, S.; Sánchez, Y.; Andrade-Arvizu, J.; Becerril-Romero, I.; Guc, M.; Giraldo, S.; Izquierdo-Roca, V.; Saucedo, E.; Sekkat, Z. Investigation on Limiting Factors Affecting $Cu_2ZnGeSe_4$ Efficiency: Effect of Annealing Conditions and Surface Treatment. *Sol. Energy Mater. Sol. Cells* **2020**, *216*, No. 110701.
(24) Ren, Y.; Richter, M.; Keller, J.; Redinger, A.; Unold, T.; Donzel-Gargand, O.; Scragg, J. J. S.; Platzer Björkman, C. Investigation of the SnS/Cu_2ZnSnS_4 Interfaces in Kesterite Thin-Film Solar Cells. *ACS Energy Lett.* **2017**, *2*, 976.
(25) Sawa, H. B.; Babucci, M.; Donzel-Gargand, O.; Pearson, P.; Hultqvist, A.; Keller, J.; Platzer Björkman, C.; Samiji, M. E.; Mlyuka, N. R. Enhanced Performance of Cu_2ZnSnS_4 Based Bifacial Solar Cells with FTO and W/FTO Back Contacts through Absorber Air Annealing and Na Incorporation. *Sol. Energy Mater. Sol. Cells* **2024**, *264*, No. 112605.
(26) Sawa, H. B.; Babucci, M.; Keller, J.; Platzer Björkman, C.; Mlyuka, N. R.; Samiji, M. E. Effects of Al_2O_3 Rear Interface Passivation on the Performance of Bifacial Kesterite-Based Solar Cells with Fluorine-Doped Tin Dioxide Back Contact. *Phys. Status Solidi (b)* **2024**, No. 2400080.
(27) Scragg, J. J.; Kubart, T.; Wätjen, J. T.; Ericson, T.; Linnarsson, M. K.; Platzer-Björkman, C. Effects of Back Contact Instability on Cu_2ZnSnS_4 Devices and Processes. *Chem. Mater.* **2013**, *25*, 3162.
(28) Sawa, H. B.; Babucci, M.; Keller, J.; Björkman, C. P.; Samiji, M. E.; Mlyuka, N. R. Toward Improving the Performance of Cu_2ZnSnS_4-Based Solar Cells with Zr, W or Sulfurized Layers at the SnO_2:F/Cu_2ZnSnS_4 Rear Interface. *Thin Solid Films* **2024**, *793*, No. 140276.
(29) Martin, N. M.; Platzer-Björkman, C.; Simonov, K.; Rensmo, H.; Törndahl, T. Passivation of CdS/Cu_2ZnSnS_4 Interface from Surface Treatments of Kesterite-Based Thin-Film Solar Cells. *Phys. Status Solidi (b)* **2020**, *257*, No. 2000308.
(30) Lindahl, J.; Hägglund, C.; Wätjen, J. T.; Edoff, M.; Törndahl, T. The Effect of Substrate Temperature on Atomic Layer Deposited Zinc Tin Oxide. *Thin Solid Films* **2015**, *586*, 82−87.
(31) Ericson, T.; Larsson, F.; Törndahl, T.; Frisk, C.; Larsen, J.; Kosyak, V.; Hägglund, C.; Li, S.; Platzer-Björkman, C. Zinc-Tin-Oxide Buffer Layer and Low Temperature Post Annealing Resulting in a 9.0% Efficient Cd-Free Cu_2ZnSnS_4 Solar Cell. *Solar RRL* **2017**, *1*, No. 1700001.
(32) Hultqvist, A.; Edoff, M.; Törndahl, T. Evaluation of Zn−Sn−O Buffer Layers for $CuIn_{0.5}Ga_{0.5}Se_2$ Solar Cells. *Prog. Photovolt. Res. Appl.* **2011**, *19*, 478.
(33) Babucci, M.; Meira, D. M.; Wallin, E.; Keller, J.; Donzel-Gargand, O.; Platzer Björkman, C.; Martin, N. M. Depth-Dependent Atomic-Scale Structural Changes in $(Ag,Cu)(In,Ga)Se_2$ Absorbers Relevant for Thin-Film Solar Cells. *ACS Appl. Energy Mater.* **2023**, *6*, 9264.
(34) *Helmholtz-Zentrum Berlin für Materialien und Energie, KMC-2: An X-Ray Beamline with Dedicated Diffraction and XAS Endstations at BESSY II*; JLSRF, 2016; Vol. 2, p A49.
(35) Ravel, B.; Newville, M. ATHENA, ARTEMIS, HEPHAESTUS: Data Analysis for X-Ray Absorption Spectroscopy Using IFEFFIT. *J. Synchrotron Rad.* **2005**, *12*, 537.
(36) Lee, T.-L.; Duncan, D. A. A Two-Color Beamline for Electron Spectroscopies at Diamond Light Source. *Synchrotron Rad. News* **2018**, *31*, 16.
(37) Li, Y.; Ling, W.; Han, Q.; Shi, W. Colloidal $Cu_2Zn(Sn_{1-x}Ge_x)S_4$ Nanocrystals: Electrical Properties and Comparison between Their Wurtzite and Kesterite Structures. *RSC Adv.* **2014**, *4*, 55016.
(38) Lafond, A.; Choubrac, L.; Guillot-Deudon, C.; Deniard, P.; Jobic, S. Crystal Structures of Photovoltaic Chalcogenides, an Intricate Puzzle to Solve: The Cases of CIGSe and CZTS Materials. *Zeitschrift für anorganische und allgemeine Chemie* **2012**, *638*, 2571.
(39) Wen, X.; Luo, W.; Guan, Z.; Huang, W.; Zou, Z. Boosting Efficiency and Stability of a Cu_2ZnSnS_4 Photocathode by Alloying Ge and Increasing Sulfur Pressure Simultaneously. *Nano Energy* **2017**, *41*, 18.
(40) *Standard X-ray Diffraction Powder Patterns*; U.S. Department of Commerce, National Bureau of Standards, 1953.
(41) Oda, K.; Nakayama, A.; Ohara, H.; Kitagawa, N.; Nomura, T. Characterization of Ion Implanted TiN Films. *Nuclear Instruments and Methods in Physics Research Section B: Beam Interactions with Materials and Atoms* **1997**, *121*, 283.
(42) Courel, M.; Sanchez, T. G.; Mathews, N. R.; Mathew, X. Cu_2ZnGeS_4 Thin Films Deposited by Thermal Evaporation: The Impact of Ge Concentration on Physical Properties. *J. Phys. D: Appl. Phys.* **2018**, *51*, No. 095107.
(43) Mora-Herrera, D.; Pal, M.; Paraguay-Delgado, F. Facile Solvothermal Synthesis of $Cu_2ZnSn_{1-x}Ge_xS_4$ Nanocrystals: Effect of Ge Content on Optical and Electrical Properties. *Mater. Chem. Phys.* **2021**, *257*, No. 123764.
(44) Parasyuk, O. V.; Piskach, L. V.; Romanyuk, Y. E.; Olekseyuk, I. D.; Zaremba, V. I.; Pekhnyo, V. I. Phase Relations in the Quasi-Binary Cu_2GeS_3−ZnS and Quasi-Ternary Cu_2S−Zn(Cd)S−GeS_2 Systems and Crystal Structure of Cu_2ZnGeS_4. *J. Alloys Compd.* **2005**, *397*, 85.
(45) Bernuy-Lopez, C.; Allix, M.; Bridges, C. A.; Claridge, J. B.; Rosseinsky, M. J. $Sr_2MgMoO_{6-\delta}$: Structure, Phase Stability, and Cation Site Order Control of Reduction. *Chem. Mater.* **2007**, *19*, 1035.
(46) Koningsberger, D. C.; Prins, R. *X-ray absorption: Principles, Applications, Techniques of EXAFS, SEXAFS and XANES*; Wiley, 1988.
(47) Baggetto, L.; Hensen, E. J. M.; Notten, P. H. L. In Situ X-Ray Absorption Spectroscopy of Germanium Evaporated Thin Film Electrodes. *Electrochim. Acta* **2010**, *55*, 7074.
(48) Zachariasen, W. H. The Crystal Structure of Germanium Disulphide. *J. Chem. Phys.* **1936**, *4*, 618.
(49) Martin, N. M.; Saini, N.; Babucci, M.; Törndahl, T.; Platzer-Björkman, C. Properties of the Interface Between the Atomic Layer Grown Zinc−Tin−Oxide and Cu_2ZnGeS_4 Relevant for Kesterite Thin-Film Solar Cells. *Phys. Status Solidi (a)* **2024**, *221*, No. 2300695.
(50) Ritzer, M.; Schönherr, S.; Schöppe, P.; Wisniewski, W.; Giraldo, S.; Gurieva, G.; Johannes, A.; Plass, C. T.; Ritter, K.; Martínez-Criado, G.; Schorr, S.; Saucedo, E.; Ronning, C.; Schnohr, C. S. On the Germanium Incorporation in $Cu_2ZnSnSe_4$ Kesterite Solar Cells Boosting Their Efficiency. *ACS Appl. Energy Mater.* **2020**, *3*, 558.
(51) Platzer-Björkman, C.; Frisk, C.; Larsen, J. K.; Ericson, T.; Li, S.-Y.; Scragg, J. J. S.; Keller, J.; Larsson, F.; Törndahl, T. Reduced Interface Recombination in Cu_2ZnSnS_4 Solar Cells with Atomic Layer Deposition $Zn_{1-x}Sn_xO_y$ Buffer Layers. *Appl. Phys. Lett.* **2015**, *107*, No. 243904.
(52) Larsson, F.; Nilsson, N. S.; Keller, J.; Frisk, C.; Kosyak, V.; Edoff, M.; Törndahl, T. Record 1.0 V Open-Circuit Voltage in Wide Band Gap Chalcopyrite Solar Cells. *Photovolt. Res. Appl.* **2017**, *25*, 755.

https://doi.org/10.1021/acsaelm.4c01317
ACS Appl. Electron. Mater. 2024, 6, 7989−7999

(53) Chen, G.; Wang, W.; Chen, S.; Whang, Z.; Huang, Z.; Zhang, B.; Kong, X. Bandgap Engineering of $Cu_2ZnSn_{1-x}Ge_xS(e)_4$ by Adjusting Sn-Ge Ratios for Almost Full Solar Spectrum Absorption. *J. Alloys Compd.* **2017**, *718*, 236.
(54) Choubrac, L.; Brammertz, G.; Barreau, N.; Arzel, L.; Harel, S.; Meuris, M.; Vermang, B. 7.6% CZGSe Solar Cells Thanks to Optimized CdS Chemical Bath Deposition. *Phys. Status Solidi (a)* **2018**, *215*, No. 1800043.
(55) Kapilashrami, M.; Kronawitter, C. X.; Törndahl, T.; Lindahl, J.; Hultqvist, A.; Wang, W.-C.; Chang, C.-L.; Mao, S. S.; Guo, J. Soft X-Ray Characterization of $Zn_{1-x}Sn_xO_y$ Electronic Structure for Thin Film Photovoltaics. *Phys. Chem. Chem. Phys.* **2012**, *14*, 10154.
(56) Mullings, M. N.; Hägglund, C.; Bent, S. F. Tin Oxide Atomic Layer Deposition from Tetrakis(Dimethylamino)Tin and Water. *J. Vacuum Sci. Technol. A: Vacuum, Surfaces Films* **2013**, *31*, No. 061503.
(57) Lee, Y. S.; Heo, J.; Siah, S. C.; Mailoa, J. P.; Brandt, R. E.; Kim, S. B.; Gordon, R. G.; Buonassisi, T. Ultrathin Amorphous Zinc-Tin-Oxide Buffer Layer for Enhancing Heterojunction Interface Quality in Metal-Oxide Solar Cells. *Energy Environ. Sci.* **2013**, *6*, 2112.
(58) Sardashti, K.; Haight, R.; Gokmen, T.; Wang, W.; Chang, L.-Y.; Mitzi, D. B.; Kummel, A. C. Impact of Nanoscale Elemental Distribution in High-Performance Kesterite Solar Cells. *Adv. Energy Mater.* **2015**, *5*, No. 1402180.

https://doi.org/10.1021/acsaelm.4c01317
ACS Appl. Electron. Mater. 2024, 6, 7989−7999